CHEMISTRY OF MATERIALS

ARTICLE

pubs.acs.org/cm

Transformation of Nano- to Mesosized Iron Oxide Cores to α-Fe within Organic Shells Preserved Intact

Shinpei Yamamoto,*[,†] Gallage Ruwan,[†,‡] Yoshinori Tamada,[§] Kaori Kohara,[†,‡] Yoshihiro Kusano,[⊥] Tatsuya Sasano,[§] Kohji Ohno,[§] Yoshinobu Tsujii,[§] Hiroshi Kageyama,[†,#] Teruo Ono,[§] and Mikio Takano[†]

[†]Institute for Integrated Cell-Material Sciences, Kyoto University, Yoshida-Ushinomiyacho, Sakyo-ku, Kyoto, 606-8501 Japan,

[‡]Toda Kogyo, Corp., 1-4, Meijishinkai, Otake, Hiroshima, 739-0652, Japan,

[§]Institute for Chemical Research, Kyoto University, Uji, Kyoto, 611-0011, Japan,

[⊥]College of the Arts, Kurashiki University of Science and the Arts, 2640 Nishinoura, Tsurajima-cho, Kurashiki-shi, Okayama 712-8505, Japan,

[#]Graduate School of Engineering, Kyoto University, Nishikyo-ku, Kyoto 615-8510, Japan

Supporting Information

ABSTRACT: Nanoparticles of α-Fe, an excellent soft magnet, have been successfully made corrosion-resistant and dispersible in polar and nonpolar solvents by coating these with inner and outer layers of amorphous silica and organics like poly(ethylene glycol), respectively. The double coating was facilitated by using stable and easy-to-handle oxide particles as the core to be subsequently metallized at temperatures low enough to keep the organic layer intact. Use of CaH_2 as a reductant lowered the working temperature down to 200−300 °C, where thermal particle adhesion did not take place, formation of impurities like iron silicates was suppressed, and the overall morphological features of the starting particles were preserved. The feasibility of organo-functionalization of the surface will open a way for this nanomagnet toward bioscientific and medical applications.

KEYWORDS: α-Fe nanoparticle, CaH_2, low-temperature reduction

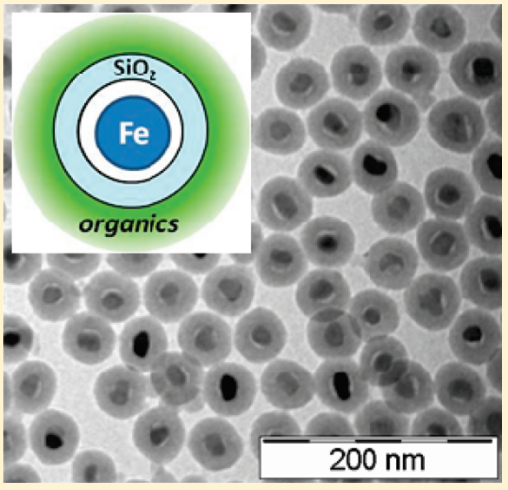

INTRODUCTION

As is well-known, α-Fe is an excellent magnet featured by a soft, large, and thermally stable magnetization. The saturation magnetization at room temperature is as large as 218 emu/g (2.2 μ_B/Fe) and, because the coercivity is so small as ∼1 × 10^{-3} T, speedy and reversible collection and dispersion of fine particles in a solvent can be done with a pocket magnet. This magnet can potentially replace oxide magnets, Fe_3O_4 (90 emu/g or 1.33 μ_B/Fe) and γ-Fe_2O_3 (76 emu/g or 1.25 μ_B/Fe), which have been most widely used for bio- and medical-sciences in the form of nano- to mesosized particles. As a matter of course, however, the metallic particles should be equipped with fortified corrosion-resistance, controllability of morphology for different uses, facile dispersibility in various solvents, and biofunctionality.[1,2]

Several groups obtained silica-coated α-Fe nanoparticles by reducing silica-coated oxide particles and showed that the metallized cores were protected from otherwise instantaneous and strongly exothermic reoxidation.[3−7] This shell material is not completely oxygen-tight because it contains open micropores. Through these pores the oxide core can release oxygen on reduction at elevated temperatures, but reoxidation through these pores after cooling is slowed kinetically. The resulting particles, however, tend to aggregate and coalesce because the normal reduction using hydrogen needs high temperatures around 450 °C. Moreover, undesirable impurities like antiferromagnetic Fe_2SiO_4 may form because of core−shell reactions at elevated temperatures.[4,7]

The most straightforward way to solve these problems is to lower the reducing temperature. We tested the reduction of iron oxide using CaH_2, which has recently acquired much attention in the field of solid state chemistry as a solid and easy-to-handle reductant working efficiently at low temperatures.[8−14] Illustrated in Scheme 1 are the ideal cases where the low-temperature reduction proceeds isotropically. Here, the overall particle shape depends on the starting oxide. After the reduction, a clearance gap opens between the core and the shell because the core volume shrinks, e.g., by 48% in the case of α-Fe_2O_3 → α-Fe.

Received: November 29, 2010
Revised: January 31, 2011
Published: February 22, 2011

Scheme 1. Schematic Representation of Synthesis of SiO_2-Coated α-Fe particles by Reducing SiO_2-Coated Iron Oxide Particles with CaH_2

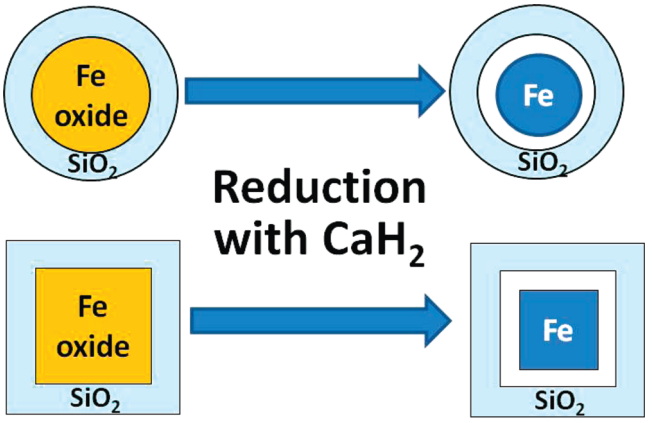

RESULTS AND DISCUSSIONS

To be shown at first are the experimental results on a pair of representative samples, A1 and A2, featuring small, round γ-Fe_2O_3 cores, and large, nearly cubic α-Fe_2O_3 cores, respectively (see Table 1). These samples were each mixed with CaH_2 powder and heated at 300 °C for 90 h in a vacuum-sealed glass tube (see Experimental Section). As can be seen in Figure 1a, the γ-Fe_2O_3 (A1) and α-Fe_2O_3 (A2) cores show different XRD patterns as a matter of course but the patterns taken after the reducing treatment are essentially the same, with three strong peaks from α-Fe. The broad peak around $2\theta = 22°$ is from the amorphous shell. This silica peak looks much stronger for A1 than for A2 for two reasons that the relative abundance of silica is much larger for A1 than for A2 and that the nanosized A1 cores show broadened peaks. The transmission electron microscopic (TEM) images taken before and after the treatment (Figure 1b, c) clearly show that the as-reduced particles keep their original overall shapes and sizes without being coalesced together. Every particle contains a single core in it normally, but rarely a few broken pieces are contained. The bright portions between the cores and the shells appearing after the reduction are the aforementioned clearance gaps. The particle viewed in Figure 1d shows lattice fringes running along a pair of orthogonal directions throughout the core. This particle may be considered to be a single crystal of α-Fe because the fringe spacing of ~0.29 nm coincides with the lattice constant of α-Fe, 0.287 nm. Then, we tried lower temperatures and found that even the large A2 particles can be metallized at 200 °C in 12 h only as Figure 1e clearly shows. If the reduction time is elongated to 7 days, the temperature can be further lowered to 180 °C for A1 (see Figure S1 in the Supporting Information).

Table 1. Mean Particle Sizes and Standard Deviations of Samples A1 and A2 before and after the reduction measured by Means of TEM[a]

sample code		A1	A2
reduction		γ-Fe_2O_3→α-Fe	α-Fe_2O_3→α-Fe
before the reduction	d_{core} (nm)	14.6 ± 2.0	[b]
	d_{all} (nm)	38.2 ± 2.1	565.4 ± 42.6
after the reduction	d_{core} (nm)	11.1 ± 2.0	374.0 ± 44.4
	d_{all} (nm)	35.9 ± 2.4	534.8 ± 55.3

[a] Here, d_{core} and d_{all} represent the core diameter and the overall particle diameter, respectively. [b] Experimental determination was prevented because the core vs shell contrast was low.

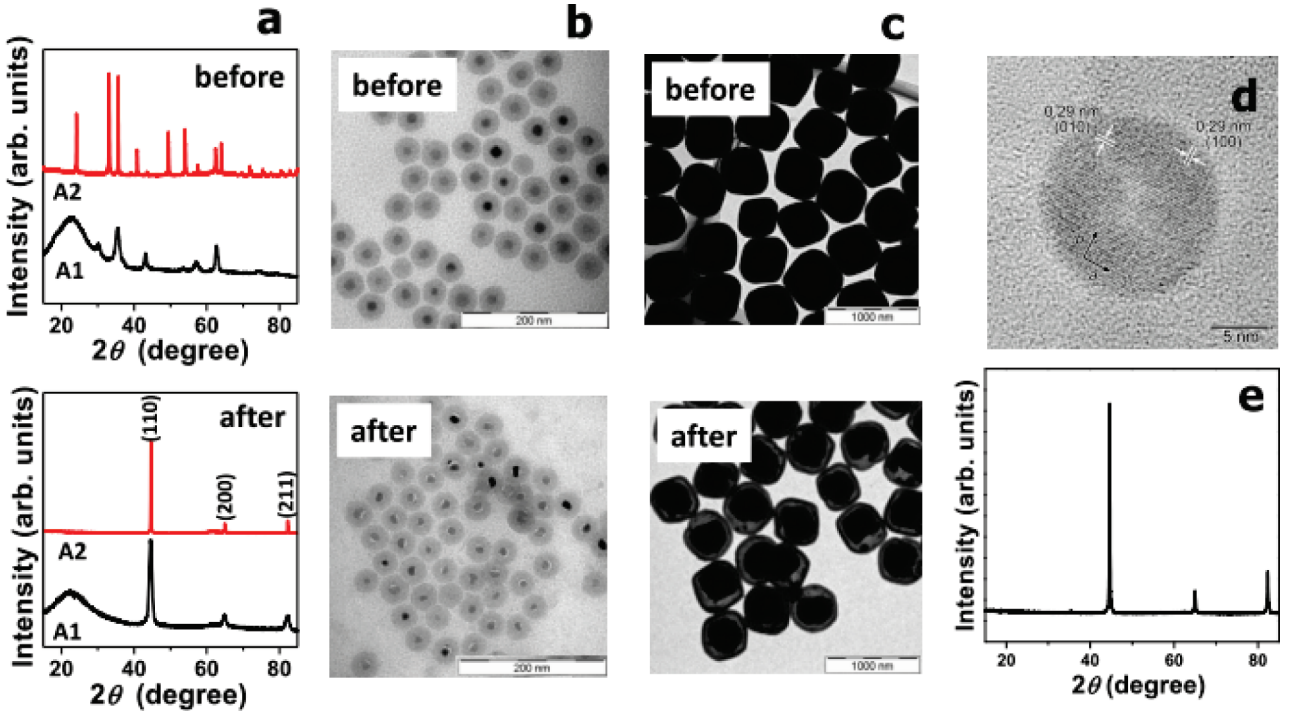

Figure 1. (a) XRD patterns before and after the reduction at 300 °C for samples A1 and A2. Low-magnification TEM images taken before and after the reduction for samples A1 (b) and A2 (c). (d) High-resolution TEM image of a particle of A1 after the reduction. (e) XRD pattern of A2 reduced at 200 °C for 12 h.

dx.doi.org/10.1021/cm103412h |*Chem. Mater.* 2011, 23, 1564–1569

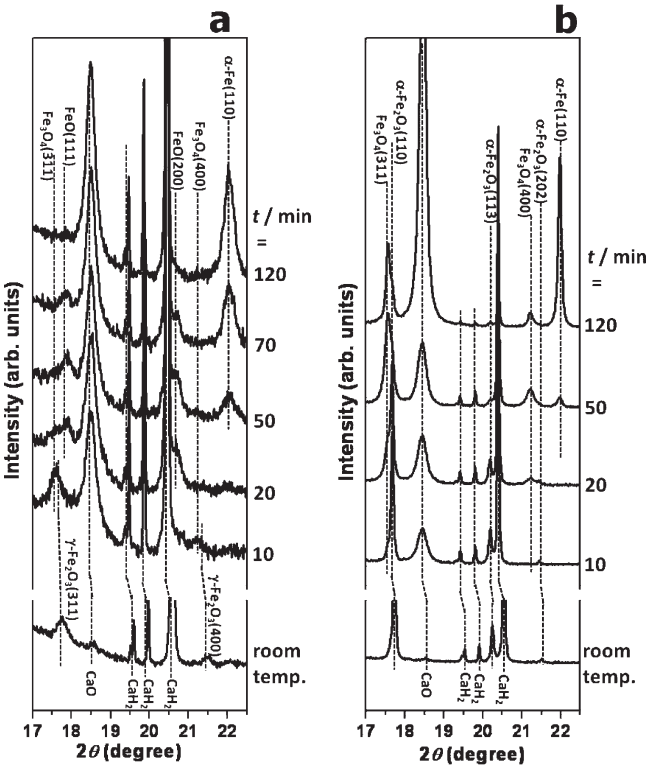

Figure 2. Time evolution of the in situ XRD profiles of (a) an A1/CaH_2 mixture measured at 300 °C and (b) an A2/CaH_2 mixture measured at 325 °C. The XRD profiles measured at room temperature before the heat treatment are also displayed at the bottom.

We traced how the reduction with CaH_2 proceeds by observing the time evolution of *in situ* synchrotron XRD patterns. Because the process is rather fast, especially for A1, the sample powder was heated up to the measuring temperature in a few seconds, and data collection over 5 min was repeated. Typical results are displayed in Figure 2, where t/min = 10, for example, indicates that the measurement was started 10 min after the initial heating followed by a thermal stabilization for 2 min and finished in 5 min. Here sample A2 shows much smoother profiles than those from A1 for the same reasons for Figure 1a. A close look at the A1 profiles shows that the starting oxide, γ-Fe_2O_3, is reduced quite rapidly to Fe_3O_4 (t/min = 10) and then to FeO (t/min = 20). α-Fe can be identified clearly in the t/min = 50 pattern. FeO and α-Fe coexist for some time, indicating that the drastic FeO → α-Fe step is more time-consuming than the oxide to oxide transformations.

Also, for sample A2 featuring large α-Fe_2O_3 cores, both the partial and complete reductions to Fe_3O_4 and α-Fe set in rather early as seen in the t/min = 20 pattern and the t/min = 50 pattern, respectively. However, in contrast to the case of A1, these three phases coexist even in the final t/min = 120 stage. Interestingly, FeO is not formed in the case of A2. It has been reported that the stability of this metastable oxide is dramatically increased in the form of nanosized particles.[15,16] It is highly possible that FeO forms only in A1 for this reason.

Here, we briefly discuss on the reduction mechanism based on the following important experimental facts. First, CaH_2 and the oxide cores are intervened by the amorphous silica shell. A likely process of oxygen transfer from the oxide core to the reductant through direct contact does not apply to the present case.

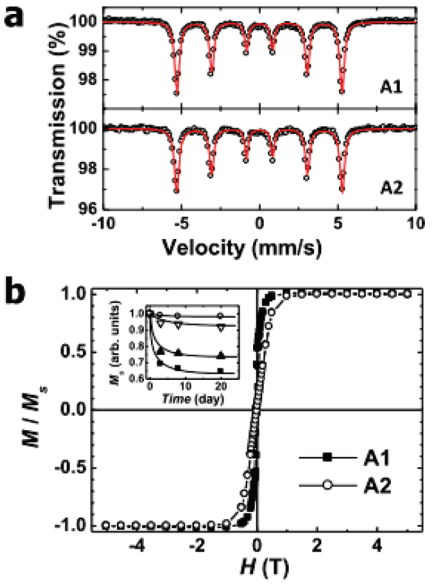

Figure 3. (a) Room-temperature Mössbauer spectra for samples A1 and A2. The open circles are the collected data and the solid lines represent the fit. (b) Room temperature hysteresis loops for the same samples. Inset shows time evolution of M_s for four samples having different core sizes which were metallized and stored in air at room temperature: 11 nm (A1, filled squares), 20 nm (filled triangles), 28 nm (open triangles), and 374 nm (A2, open circles).

Table 2. Mössbauer Hyperfine Values at 300 K[a]

	CS (mm/s)	HF (T)	QS (mm/s)	fwhm (mm/s)
A1	0	32.7	0	0.32
A2	0	32.8	0	0.32

[a] Here, CS, HF, QS, and fwhm represent center shift relative to α-Fe at 300 K, magnetic hyperfine field, quadrupole splitting, and full width at half maximum, respectively.

Second, the metallization proceeds even at such a low temperature of 180 °C. CaH_2, when it is free, is known to be decomposed to calcium metal and hydrogen at about 600 °C. The contact with silica might possibly facilitate this decomposition drastically and the hydrogen thus released might work as a reductant. Experimentally, however, we did not detect calcium metal at all by the in situ XRD measurements (Figure 2). Further, it is known that even flowing hydrogen stream cannot metallize iron oxides at such a low temperature of 200−180 °C. We thus think that the driving force of the present low temperature reduction is the great stability of CaO, not the stability of H_2O. In other words, CaH_2 is a very powerful oxygen getter that takes oxygen from the oxide cores through the open pores of silica at the expense of hydrogen release. Experimentally, CaO was found to form in the initial heating step and increase with time in the in situ XRD patterns.

Magnetic properties of the metallized samples were studied macroscopically and microscopically by means of SQUID magnetometry and ^{57}Fe Mössbauer spectroscopy, respectively. Presented in Figure 3a are the room-temperature Mössbauer spectra of the reduced A1 and A2. Both these spectra could be computer fitted by a single magnetically split pattern, and the hyperfine parameters were found to coincide with those of α-Fe bulk within experimental error (see Table 2). Likely impurities

dx.doi.org/10.1021/cm103412h |*Chem. Mater.* 2011, 23, 1564–1569

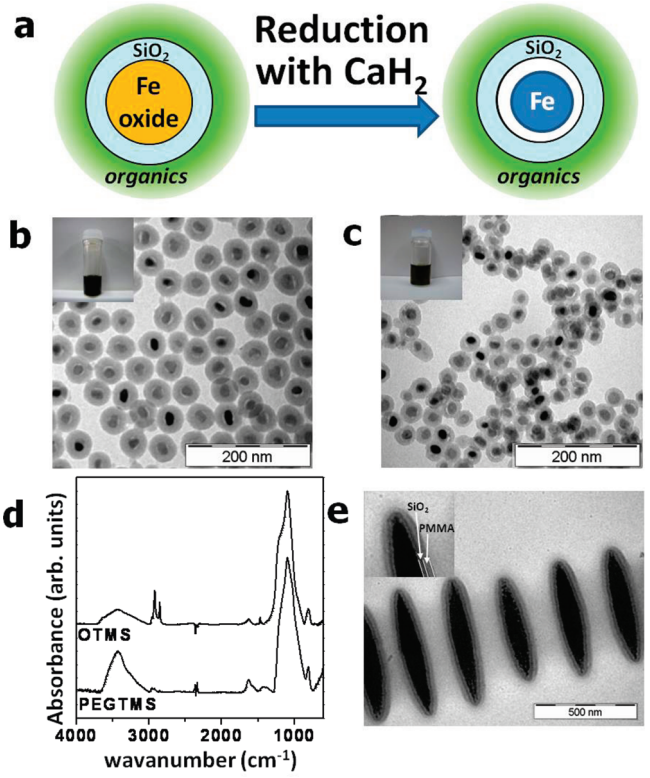

Figure 4. (a) Schematic representation of the reduction of iron oxide-core/SiO_2 shell/organic shell particles. (b) Low-magnification TEM image of OTMS-modified sample taken after the reduction. Inset shows a dispersed sample in chloroform. (c) Low-magnification TEM image of PEGTMS-modified sample taken after the reduction. Inset shows a dispersed sample in water. (d) IR spectra of the samples modified with OTMS and PEGTMS after the reduction. (e) Low-magnification TEM image of spindle-shaped SiO_2/α-Fe_2O_3 particles coated with PMMA taken after the reduction at 200 °C for 5 days. Inset shows a magnified view showing the inner (SiO_2) and outer (PMMA) coating layers.

including residual starting oxides, silicates, partially reduced oxides such as Fe_3O_4 and FeO, and very fine superparamagnetic α-Fe particles to show a single absorption peak are all absent. Figure 3b shows their magnetic hysteresis loops measured at room temperature. Here, M_s represents the magnetization at 5 T. Both these samples quickly increase and decrease their magnetization between $+M_s$ and $-M_s$ with a small coercivity of 0.025 T (A1) to 0.005 T (A2), as expected from the softness of α-Fe. From the aforementioned Mössbauer results we may expect that the real magnitude of magnetization should coincide to the bulk value of 218 emu/g. Actually, the M_s of A2 particles reduced at 250 °C for 96 h was found to be 2.1×10^2 emu/g Fe. The determination of iron content needed for this estimation was done by using an inductively coupled plasma optical emission spectrometer, whereas the precision was lost for the silica-abundant sample like A1.

The stability against oxidation in air at room temperature was studied for four samples having different core sizes through intermittent magnetization measurements over 20 days (see inset of Figure 3b). The decrease in M_s due to reoxidation ranged from just 2% for A2 to 35% for A1 after 20 days. The decrease is not monotonous and almost ceases in ~7 days. A metal-core/oxide-shell structure seems to be stabilized. If it is assumed that the oxidized layer is Fe_3O_4 with an ideal saturation magnetization of 90 emu/g and that the moment is coupled parallel to that of the core, the thickness is calculated to be 1.1 nm (49 vol %) and 1.5 nm (2 vol %) for A1 and A2, respectively. Experimentally, some very broad XRD peaks likely assigned to Fe_3O_4 appeared but details are yet to be investigated. We note here that the real oxidized layers must be considerably thinner than calculated above because poorly crystallized magnetite cannot have such a large magnetization.

Suppose the starting silica/iron-oxide particles are overcoated with an organic layer as illustrated in Figure 4a. If the organic molecules could remain intact through the thermal treatment for reduction, the resulting composite will immediately exhibit the given organo-functionality. We first tried model cases of octadecyltrimethoxysilane (OTMS) and poly(ethylene glycol) (PEG)-carrying silane-coupling agent (PEGTMS). Images b and c in Figure 4 show typical TEM images taken after the reduction at 300 °C for 90 h, which look essentially the same as nonovercoated particles shown in Figure 1. The formation of well-crystallized α-Fe was confirmed by XRD measurement (see Figure S2 in the Supporting Information). The organic layers of less than 2 nm thick each could not be identified by XRD or TEM but their balanced existence was confirmed through infrared spectroscopy (IR). The absorption peaks at around 2900 cm^{-1} seen in Figure 4d are from these molecules. Actually this enabled facile and stable dispersion of the as-reduced particles. Bottled dispersions of the OTMS-coated sample in chloroform and the PEGTMS-coated sample in water are shown in insets of Figures 4b and 4c, respectively. We should emphasize here that these stable dispersions can be readily prepared even from vacuum-dried and stored sample powder. The pegylated, potentially biocompatible[17] α-Fe particles forms a stable dispersion in phosphate-buffered saline, the use tests of which for magnetic resonance imaging and hyperthermia are currently under way.

The range of available organic compounds can be expanded if the core reduction can be done at lower temperatures. We tested the case of poly(methyl methacrylate) (PMMA) which is known to decompose rapidly at 300 °C. Figure 4e shows a TEM image of spindle-shaped silica/α-Fe_2O_3 particles overlayered with PMMA and metallized at 200 °C for 5 days. Both the inner silica shell and the outer PMMA shell can be clearly identified in the enlargement. The presence of PMMA was confirmed through facile and stable dispersion in chloroform (see Figure S3 in the Supporting Information).

■ CONCLUSION

The use of CaH_2 as a reductant provides a way to obtain nano- to meso-sized particles of α-Fe equipped with fortified corrosion resistance, facile dispersibility, controlled morphology, and organo-functionality. This success may open a way for this excellent magnet toward bioscientific and medical applications. The fabrication process starts with double-coating of iron oxides with amorphous silica and organic compounds. The subsequent low-temperature reduction has been thought to be driven by the great stability of CaO, not that of H_2O.

■ EXPERIMENTAL SECTION

Preparation of Silica-Coated γ-Fe_2O_3 Nanoparticles (A1). The silica-coated γ-Fe_2O_3 nanoparticles were prepared according to the procedures described elsewhere.[7] In brief, γ-Fe_2O_3

dx.doi.org/10.1021/cm103412h |Chem. Mater. 2011, 23, 1564–1569

nanoparticles with an average particle size of 14.6 nm were prepared[18] and the SiO_2 coating was performed through the formation of water-in-cyclohexane reverse microemulsion.[19] To the cyclohexane solution (48.75 g) containing polyoxyethylene(5)nonylphenyl ether (3.65 g, 8.3 mmol) and the γ-Fe_2O_3 nanoparticles (0.1 g), ammonium hydroxide (28%, 0.39 mL) was added and magnetically stirred for 30 min to form a transparent, brown solution of reverse microemulsion. Tetraethyl orthosilicate (0.4 g, 1.9 mmol) was then added, and the reaction was continued for 18 h at room temperature. The silica-coated γ-Fe_2O_3 nanoparticles were precipitated by adding ethanol to the reaction solution. They were collected by a magnet, washed with ethanol, and dried in a vacuum.

Preparation of Silica-Coated α-Fe_2O_3 Particles (A2). Cubic α-Fe_2O_3 particles were synthesized according to the procedures described elsewhere[20] and then coated with silica through hydrolysis of tetraethoxyorthosilicate in ethanol/water mixture (Stöber method). In brief, α-Fe_2O_3 particles were first prepared by forced hydrolysis of mixed solution of $FeCl_3$ (3.12×10^{-2} mol dm^{-3}) and HCl (9.60×10^{-3} mol dm^{-3}) with polyvinyl alcohol (MW= 22000, 0.0003 wt %) in Teflon lined autoclave (100 mL) in conventional oven at 105 °C. Hydrothermal treatments were conducted for 7 days and the precipitate was separated by centrifuging followed by washing with distilled water (3 times). Finally, powder samples were dried at 60 °C for 24 h. Next, α-Fe_2O_3 particles (100 mg) were dispersed in three neck flask containing mixed solution of ethanol (200 mL), water (15 mL), and ammonium hydroxide (28%, 3 mL). The flask was placed in an Ultrasonicator coupled with mechanical stir. While stirring and sonication proceeded, 4 mL of TEOS in ethanol (3.2% by volume) was injected into the suspension at a rate of 500 μL/h using an injection pump. At the end of adding TEOS, continue the stirring and sonication for another 12 h. Finally, particles were washed three times with ethanol followed by centrifuging and dried at room temperature.

Surface Modification of Silica-Coated Iron Oxide Nanoparticles. The OTMOS-modification was performed by adding OTMOS to the reaction solution for SiO_2 coating. After formation of the silica-coated iron oxide nanoparticles, OTMOS was directly added to the reaction solution (OTMS/solution = 0.1/10 in weight) and keeping it for 3 days. The OTMOS-modified samples were precipitated by adding ethanol to the reaction solution. They were collected by a magnet, washed with ethanol, and dried in vacuum. The PEGTMS-modification was performed based on the procedures described elsewhere.[21] As the PEG-carrying silane-coupling agent (PEGTMS), 2-[methoxy(polyethyleneoxy)propyl]trimethoxysilane was used. In brief, silica-coated iron oxide nanoparticles were dispersed in ethanol (50 mL) followed by the addition of PEGTMS (2 g). The above mixture was stirred for 6 h at 80 °C. The PEGTMS-modified samples were collected by a magnet, washed with ethanol, and dried in a vacuum.

Preparation of Spindle-Shaped Silica/α-Fe_2O_3 Particles Coated with PMMA. Spindle-shaped silica/α-Fe_2O_3 particles coated with PMMA were prepared as follows: The spindle-shaped α-Fe_2O_3 nanoparticles were synthesized according to the procedures described elsewhere[22] and coated with silica by the Stöber method. Living radical graft polymerization of methyl methacrylate was then performed on the surface of silica with an initiator fixed on it.

Reduction with CaH_2. The reduction was done according to the method described in elsewhere.[11] In brief, a silica-coated sample and a four-weight excess of CaH_2 were finely ground in an Ar-filled glovebox, sealed in an evacuated Pyrex tube, and heated at various temperatures and for various reaction times. Before preparation of the reaction mixture, the silica-coated samples were dried under a vacuum. Residual CaH_2 and CaO produced during the reduction were washed out with an NH_4Cl/methanol solution in an Ar-filled glovebox.

in situ XRD Measurement. in situ XRD measurements were done for 5 min each using a beamline BL02B2 of SPring-8 (λ = 0.07750 nm) equipped with a large Debye−Scherrer camera with an imaging plate as a detector. The starting silica-coated oxide particles mixed with CaH_2 and sealed in glass capillaries under an Ar atmosphere were heated up quickly (within a few seconds) and the measurements were started after a thermal stabilization for 2 min. Also for these measurements two- and four-weight excess of CaH_2 were employed to A1 and A2, respectively.

Characterization Methods. Low- and high-resolution TEM observations were performed by using a JEOL JEM-1010D and a JEOL JEM-4000EX, respectively. TEM specimens were prepared by dropping the particle-containing solution on a carbon-coated copper grid. XRD measurements were performed using a Rigaku RINT2500 with Cu K_α radiation (λ = 0.154 nm). ^{57}Fe Mössbauer measurements were performed at 300 K in transmission geometry using a radioactive source of ^{57}Co in Rh matrix in a constant acceleration mode. Macroscopic magnetic properties were characterized by using a SQUID magnetometer (Quantum Design MPMS XL). Elemental analysis was performed by using an inductively coupled plasma optical emission spectrometer (ThermoFischer Scientific, iCAP 6300DUO). IR spectra were collected on a BioRad FTS-6000 and a JASCO FT/IR-4200. The samples were mixed with KBr and compressed into pellets.

■ ASSOCIATED CONTENT

Supporting Information. XRD pattern of A1 reduced at 180 °C (Figure S1), XRD patterns of OTMOS- and PEGTMS-coated samples after reduction (Figure S2), and photographs of dispersion of spindle-shaped particles (Figure S3) (PDF). This material is available free of charge via the Internet at http://pubs.acs.org.

■ AUTHOR INFORMATION

Corresponding Author

*E-mail: yamamoto@icems.kyoto-u.ac.jp. Phone: +81-75-753-9772. Fax: +81-75-753-9785.

■ ACKNOWLEDGMENT

This work was supported in part by Adaptable and Seamless Technology Transfer Program through Target-driven R&D, JST, MEXT KAKENHI (20104006) and the iCeMS Exploratory Grants for Junior Investigators.

■ REFERENCES

(1) Huber, D. L. *Small* **2010**, *1*, 482–501.
(2) Lu, A.-H.; Salabas, E. L.; Schüth, F. *Angew. Chem., Int. Ed.* **2007**, *46*, 1222–1244.
(3) Hisano, S.; Saito, K. *J. Magn. Magn. Mater.* **1998**, *190*, 371–381.
(4) Tartaj, P.; Serma, C. J. *J. Am. Chem. Soc.* **2003**, *125*, 15754–15755.
(5) Ohimori, M.; Matijević, E. *J. Colloid Interface Sci.* **1993**, *160*, 288–292.
(6) Zhao, W.; Gu, J.; Zhang, L.; Chen, H.; Shi, J. *J. Am. Chem. Soc.* **2005**, *127*, 8916–8917.
(7) Inoue, T.; Tamada, Y.; Yamamoto, S.; Nasu, S.; Ono, T. *J. Magn. Soc. Jpn.* **2008**, *32*, 321–324.
(8) Hayward, M. A.; Cussen, E. J.; Claridge, J. B.; Bieringer, M.; Rosseinsky, M. J.; Kiely, C. J.; Blundel, S. J.; Marshall, I. M.; Pratt, I. L. *Science* **2002**, *295*, 1882–1884.
(9) Blundred, G. D.; Bridges, A. B.; Rosseinsky, M. J. *Angew. Chem., Int. Ed.* **2004**, *43*, 3562–3565.
(10) Bowman, A.; Allix, M.; Pelloquin, D.; Rosseinsky, M. J. *J. Am. Chem. Soc.* **2006**, *128*, 12606–12607.

(11) Tsujimoto, Y.; Tassel, C.; Hayashi, N.; Watanabe, T.; Kageyama, H.; Yoshimura, K.; Takano, M.; Ceretti, M.; Ritter, C.; Paulus, W. *Nature* **2007**, *450*, 1062–1065.
(12) Kageyama, H.; Watanabe, T.; Tsujimoto, Y.; Kitada, A.; Sumida, Y.; Kanamori, K.; Yoshimuar, K.; Hayashi, N.; Muranaka, S.; Takano, M.; Ceretti, M.; Paulus, W.; Ritter, C.; André, G. *Angew. Chem., Int. Ed.* **2008**, *47*, 5740–5745.
(13) Tassel, C.; Pruneda, J. M.; Hayashi, N.; Watanabe, T.; Kitada, A.; Tsujimoto, Y.; Kageyama, H.; Yoshimura, K.; Takano, M.; Nishi, M.; Ohoyama, K.; Mizumaki, M.; Kawamura, N.; Íniguez, J.; Canadell, E. *J. Am. Chem. Soc.* **2009**, *131*, 221–229.
(14) Inoue, S.; Kawai, M.; Ichikawa, N.; Kageyama, H.; Paulus, W.; Shimakawa, Y. *Nature Chem.* **2010**, *2*, 213–217.
(15) Redl, F. X.; Black, C. T.; Papaefthymiou, G. C.; Sandstrom, R. L.; Yin, M.; Zeng, H.; Murray, C. B.; O'Brien, S. P. *J. Am. Chem. Soc.* **2004**, *128*, 14583.
(16) Hou, Y.; Xu, Z.; Sun, S. *Angew. Chem., Int. Ed.* **2007**, *46*, 6329.
(17) Harris, J. M.; Chess, R. B. *Nat. Rev. Drug Delivery* **2003**, *2*, 214–221.
(18) Park, J.; An, K.; Hwang, Y.; Park, J.-G.; Noh, H.-J.; Kim, J.-Y.; Park, J.-H.; Hwang, N.-M.; Hyeon, T. *Nat. Mater.* **2004**, *3*, 891–895.
(19) Yi, D. K.; Lee, S. S.; Papaefthymiou, G. C.; Ying, J. Y. *Chem. Mater.* **2006**, *18*, 614–619.
(20) Kandori, K.; Hori, N.; Ishikawa, T. *Colloid Polym. Sci.* **2006**, *284*, 1345–1349.
(21) Chandran, S. P.; Hotha, S.; Prasad, B. L. V. *Curr. Sci.* **2008**, *95*, 1327–1333.
(22) Ozaki, M.; Kratohvil, S.; Matijević, E. *J. Colloid Interface Sci.* **1984**, *102*, 146–151.